Improving radiation hardness in space-based Charge-Coupled Devices through the narrowing of the charge transfer channel

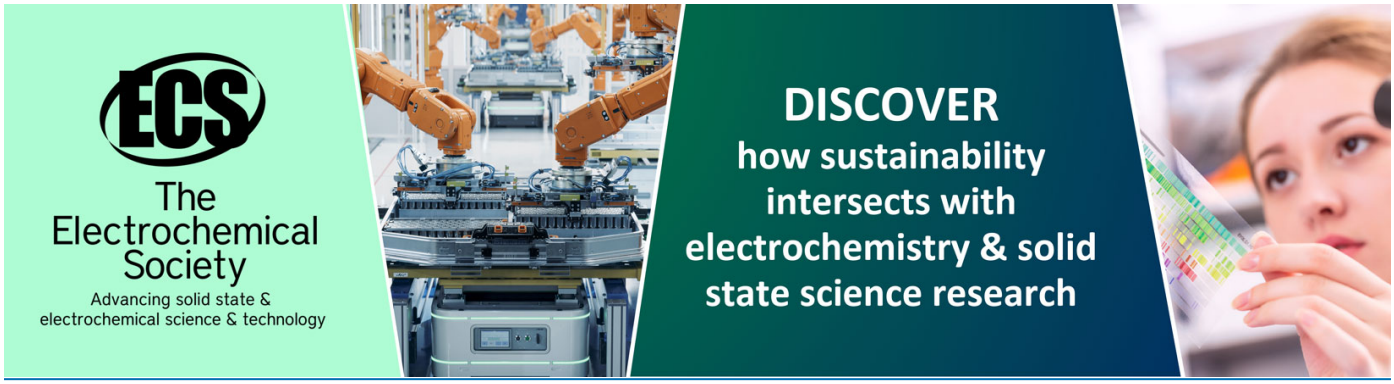

Jinst

Published by IOP Publishing for Sissa Medialab

Received: *October 24, 2017*
Accepted: *November 8, 2017*
Published: *December 12, 2017*

11TH International Conference on Position Sensitive Detectors
3–8 September 2017
The Open University, Walton Hall, Milton Keynes, U.K.

Improving radiation hardness in space-based Charge-Coupled Devices through the narrowing of the charge transfer channel

D.J. Hall,[1] J. Skottfelt, M.R. Soman, N. Bush and A. Holland

Centre for Electronic Imaging, The Open University,
Walton Hall, Milton Keynes, MK7 6AA, U.K.

E-mail: david.hall@open.ac.uk

Abstract: Charge-Coupled Devices (CCDs) have been the detector of choice for imaging and spectroscopy in space missions for several decades, such as those being used for the Euclid VIS instrument and baselined for the SMILE SXI. Despite the many positive properties of CCDs, such as the high quantum efficiency and low noise, when used in a space environment the detectors suffer damage from the often-harsh radiation environment. High energy particles can create defects in the silicon lattice which act to trap the signal electrons being transferred through the device, reducing the signal measured and effectively increasing the noise.

We can reduce the impact of radiation on the devices through four key methods: increased radiation shielding, device design considerations, optimisation of operating conditions, and image correction. Here, we concentrate on device design operations, investigating the impact of narrowing the charge-transfer channel in the device with the aim of minimising the impact of traps during readout.

Previous studies for the Euclid VIS instrument considered two devices, the e2v CCD204 and CCD273, the serial register of the former having a 50 μm channel and the latter having a 20 μm channel. The reduction in channel width was previously modelled to give an approximate 1.6× reduction in charge storage volume, verified experimentally to have a reduction in charge transfer inefficiency of 1.7×. The methods used to simulate the reduction approximated the charge cloud to a sharp-edged volume within which the probability of capture by traps was 100%. For high signals and slow readout speeds, this is a reasonable approximation. However, for low signals and higher readout speeds, the approximation falls short.

Here we discuss a new method of simulating and calculating charge storage variations with device design changes, considering the absolute probability of capture across the pixel, bringing

[1]Corresponding author.

https://doi.org/10.1088/1748-0221/12/12/C12021

validity to all signal sizes and readout speeds. Using this method, we can optimise the device design to suffer minimum impact from radiation damage effects, here using detector development for the SMILE mission to demonstrate the process.

KEYWORDS: Detector modelling and simulations I (interaction of radiation with matter, interaction of photons with matter, interaction of hadrons with matter, etc); Photon detectors for UV, visible and IR photons (solid-state) (PIN diodes, APDs, Si-PMTs, G-APDs, CCDs, EBCCDs, EMCCDs etc); Radiation damage evaluation methods; Radiation-hard detectors

2017 JINST 12 C12021

Contents

2017 JINST 12 C12021

1 Introduction

Charge-Coupled Devices (CCDs) are often used as the focal plane detectors for space missions and as such may suffer from the harsh radiation environment of the mission's orbit. When an energetic charged particle, such as a high energy proton (found to dominate the radiation environment for many mission orbits), traverse the detectors they can effectively knock a silicon atom from the uniform lattice structure. The resulting "vacancy" (absence of silicon atom) is inherently unstable and will migrate through the lattice structure until it is able to form a more stable structure such as a divacancy (formed from two vacancies in neighbouring lattice sites) or a Silicon A-centre (a vacancy and an oxygen atom). The stable defects in the lattice create additional energy levels between the valence and conduction bands in the silicon. These additional energy levels form "traps" that can capture the signal electrons as they are transferred through the CCD, only releasing them at a later point in time determined by the trap emission time constant; it is these traps that cause a reduction in the Charge Transfer Efficiency (CTE) and cause the loss of charge and/or smearing of images from spaceborne CCDs. The capture and release of electrons by traps is described well by Shockley-Read-Hall theory [1, 2], with an exponential time constant determining the probability of capture and emission by each trap. Further details of how Shockley-Read-Hall theory can be applied to the capture and emission of electrons by traps in a CCD can be found in [3].

If trap sites are uniformly distributed throughout the silicon lattice within the CCD then a trap density can be defined in units of traps per unit volume. If one considers a "charge cloud" of signal electrons being transferred through the CCD during readout then, to a first approximation, the amount of charge lost from that charge cloud will be proportional to the number of traps encountered

and hence the volume of the charge cloud. If the volume of the charge cloud could be reduced then it would be reasonable to expect that the amount of charge lost would also be reduced.

The propotionality of charge loss to charge cloud size is in fact a fairly good approximation for slow moving charge clouds that contain a large number of signal electrons . The approximation is reasonable in this case because the density of the charge cloud for large signals, coupled with the long dwell times caused by the slow readout, means that the probability of capture is approximately (or very close to) one across the whole charge cloud [4].

One way to reduce the volume of such a charge cloud is through the reduction of the width of the buried channel or the electrodes in the device. This reduction along one axis must be considered with caution, however, because the charge cloud may behave in a similar manner to an inflated balloon; if the balloon is squashed along one axis then there may be an increase in size along an orthogonal axis, i.e. a reduction in width of the buried channel by a factor of two is unlikely to lead to a reduction in the charge cloud volume by a factor of two. In section 3 we consider the case of the Euclid CCD in more detail, demonstrating this effect.

So far we have only considered a slow-moving (of the order of tens of milliseconds), high-signal charge cloud (of the order of tens of thousands of electrons), such that the high charge density across the charge cloud and the long dwell times result in a probability of capture of close to one across the whole charge cloud volume. In the case of a lower signal and quicker transfer, such as that proposed for the Solar wind Magnetosphere Ionosphere Link Explorer (SMILE) mission [5], a joint mission between the European Space Agency (ESA) and the Chinese Academy of Sciences, the approximations discussed above do not hold. If the electron density within the charge cloud coupled with the dwell time results in a probability of capture below one, then the change in size of the charge cloud in one dimension, coupled with the resultant changes in cloud size in the two orthogonal directions, can cause a variation in the capture probability across the cloud. This variation in capture probability gives the possibility that a reduction in the size of the charge cloud could, in fact, cause an increase in the overall probability of capture across the charge cloud in certain conditions. For such cases, a thorough investigation is required to ensure the device is optimised appropriately for the application.

2 Mitigation strategies

As the science requirements for space missions increasingly become more demanding, the requirements placed on the detectors also become more challenging. As we look towards fainter and fainter objects in the sky alongside the desire to observe over larger areas, the decreased signal and larger detectors (meaning more silicon to traverse) act to magnify the impact of radiation damage. In order to counteract the increasingly challenging demands on the radiation hardness required by a device (or minimise the impact of radiation on the ability to achieve the science goals), four key methods can be considered:

- Radiation shielding: reduce the dose of radiation at the device through increased shielding (section 2.1).
- Device design optimisation: optimise the design of the device to minimise the impact of any radiation damage suffered (section 2.2).

2017 JINST 12 C12021

- Operating conditions: operate the device in such a way as to minimise the impact of radiation damage (section 2.3).
- Image correction: correct images during post-processing to remove the effects of the radiation damage (section 2.4).

2.1 Radiation shielding

If a CCD was to be placed within a space radiation environment with no protection, then the damage caused by lower energy protons would quickly create too many traps for a reasonable image to be read out. Behind a radiation shield, which may be formed from the spacecraft itself, the lower energy protons are attenuated and the radiation spectrum *inside* of the shielding is reduced in flux. However, with an increase in the shielding, an increase in the flux of secondary particles and X-rays (i.e. those released or generated inside the shielding from the incident primary particles) may be observed. These secondaries can, in some cases, cause more damage to the detector than the incident primaries. The main concern, however, with increased secondary particle generation is an increase in instrument background. Instrument background can be described as the background observed by the detector that looks like, for example, the X-ray events that one is trying to observe, but is not caused by X-rays passing through the telescope optics, i.e. false events recorded in the detector due to interactions in the material surrounding the detector. It has been demonstrated for ESA's XMM-Newton mission that such background can be simulated well using Monte Carlo simulations such as those performed with Geant4 [6].

Whilst the radiation damage can be reduced through effective shielding design, the increased instrument background must also be considered. Methods being considered to minimise the instrument background for ESA's Advanced Telescope for High ENergy Astrophysics (ATHENA) mission include the use of graded-Z shielding; through using materials with ever reducing atomic number, secondary events such as X-ray fluorescence, can be removed from the energy range of interest [7].

2.2 Device design optimisation

The second method that we consider here is that of optimising the design of the device. Whilst various steps can be taken to optimise the device, the two most common are that of reducing the volume in which charge is stored and/or transferred, which we will consider further in section 3, and that of the device surface structures. For example, through the use of thinner oxides, charge build-up that causes the change of flat-band voltage can be reduced [8]. One might also consider the use of a p-channel CCD rather than the more common n-channel CCD; by using a device that generates signal in the form of holes rather than electrons, the signal charge will effectively encounter a different trap landscape (different trap emission times at any particular temperature) due to being susceptible to those trapping sites with energies close to the valence band rather than the conduction band. Thus, in some cases, the p-channel CCD may be considered more radiation hard than an n-channel CCD [9, 10].

2.3 Operating conditions

The impact of radiation damage can be dramatically reduced through the appropriate choice of operating conditions for the device and application. The traps that interfere with the charge transfer,

2017 JINST 12 C12021

if well known, can be avoided (or at least their impact reduced) through appropriate choice of operating temperature and clock transfer timings.

For example, operating at a warmer temperature may speed up the emission time of a trap such that more trapped charge is emitted back into the charge packet from which it was captured (resulting in no net charge loss). In other cases, running cooler may be beneficial in keeping traps that have captured filled for longer, allowing other signal charge to pass by the trap (which will not capture if it is already full).

In terms of clock timings, adjusting the time between transfers from one pixel to the next (in fact, from one electrode to the next) can provide major benefits against the effects of radiation damage. Early studies towards ESA's Euclid mission found a factor of three variation between the so-called 'video' mode (transferring very quickly from one parallel pixel to the next with a long waiting time during readout) and a more even clocking mode (moving more slowly through the pixel) [3]. The optimal clocking scheme to minimise the probability of charge being deferred from one pixel to the next was found to be achieved through "even" clocking (keeping the charge under each electrode for the same amount of time) [3], however, any changes in the transfer timings should be balanced against any change in the readout noise from adjusting the time available to sample the charge at the output.

The above-mentioned methods require an understanding of the trap species present in the device. Whilst one can find approximate bulk values for traps species through analysing the change in Charge Transfer Inefficiency (CTI) with timings and temperature, the method of "trap pumping" allows individual traps to be probed in the device [11], leading to the development of a method to determine the properties of individual traps in the device [12]. Through analysing each individual trap, much greater detail can be found about the time constants for populations of traps [10, 12–14]. Using these detailed maps of the trap populations in the device, the ability to avoid the dominant trap species is greatly improved.

2.4 Image correction

Once all of the previously mentioned methods have been considered and a device is in flight, the images that are returned may still suffer some effects from radiation damage. This damage can, to a certain extent, be corrected against in software.

One such method that has been used successfully for the Hubble Space Telescope (HST) involves the simulation of further radiation damage on the damaged image received from the telescope [15, 16]. By adding additional charge trailing and subtracting multiples of the original image, one can get close to the undamaged image that was intended to be observed. The method relies upon the accuracy of the simulation for the additional radiation damage to be added to the images; ultimately the more realistic the simulation, the better the correction achieved. For cases where increased correction is required, knowledge of the trap population is required in fine detail and methods such as the trap pumping technique discussed in section 2.3 can be of great importance.

3 CCD design optimisation for Euclid

Towards ESA's Euclid mission, specifically the VIS instrument, simulations were implemented to calculate the expected improvement in charge transfer efficiency through the use of a narrow serial

2017 JINST 12 C12021

channel [4, 17, 18]. The initial devices, the e2v CCD204 [19], were produced with a 50 μm serial channel. Through a reduction in the serial channel width to 20 μm (a factor 2.5 reduction) in the e2v CCD273 [19], the CTE was expected to improve. As discussed previously, however, one would not expect a factor 2.5 improvement in CTE, as the charge packet acts in a similar way to a balloon that is being squashed along one axis, i.e. the volume does not scale linearly with the reduction in width.

Using the Silvaco toolkit [20], the two device geometries were simulated. Placing an electron charge cloud in the serial register of the device at many different signal levels, the variation in volume of the charge packet (and therefore the expected interaction with traps) was estimated. The method used in these early studies [4, 17, 18, 21] was optimised for use in this case with larger signal levels and slower transfer speeds. For these conditions, the probability of capture by a trap in any position within the charge cloud is close to one, such that the volume of the charge packet can be approximated by measuring the position of the relatively sharp drop in electron density at the edges of the charge cloud and assuming a probability of capture of one within these boundaries, figure 1 and figure 2. Using this method, a factor 1.6 to 2.6 reduction in CTE was predicted (moving from one million electrons in the charge cloud to one electron in the charge cloud respectively) [18]. This simulated result was later verified experimentally with a factor 1.7 improvement in X-ray CTE measured at 5898 eV (approximately 1600 electrons), within 10% of the simulated value [4].

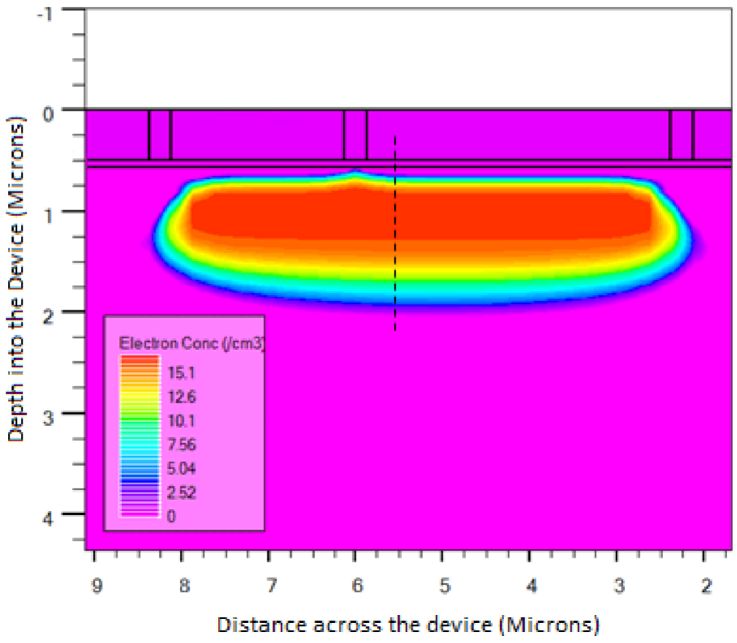

Figure 1. A side-on view of the electron density from a cut-plane through the pixel (adapted from [18] © IOP Publishing Ltd. All rights reserved).

Problems arise with the method discussed above if the signal level is low or the charge cloud is transferred more quickly through the device; with a low charge density and short dwell time the probability of capture can be reduced much below one such that the charge packet can no longer be considered as having a well-defined "edge". In these cases, a more detailed approach is required.

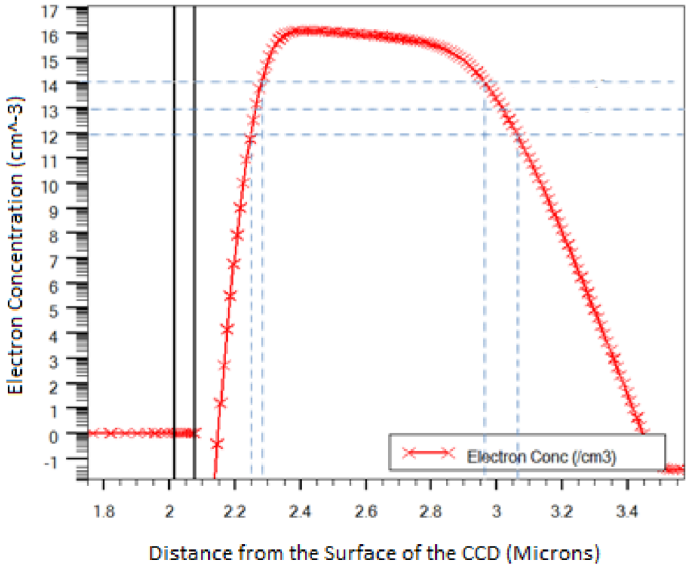

Figure 2. The profile of the electron concentration shown in figure 1 along the black dashed line, vertically through the device, showing the sharp rises in density to the maximum values, noting the logarithmic y-axis (adapted from [18] © IOP Publishing Ltd. All rights reserved).

4 A more detailed approach to charge storage modelling

The probability of a signal electron being captured by a trap is not determined only by the presence of the charge cloud within its vicinity, but by the electron density at that position. In such a way, the probability of capture by a trap can vary dramatically across the signal charge cloud and it is the total probability of capture across the entire charge cloud that plays a major role in determining the CTE. In an extreme example, one might consider that restricting the charge cloud to a smaller volume might increase the electron density such that the probability of capture could in fact increase. It is for this reason that a new method has been developed to simulate and test new device structures before the costly process of going through manufacture.

Rather than using the instantaneous trapping approximation, as used in the method previously described, we now consider the electron density across the whole cloud when calculating the probability of capture of an electron by a trap. A fine, uniform mesh is generated across the buried channel of the device across the pixel. At each mesh point, the electron density is interpolated from the Silvaco simulations. Noting the dwell time for the clocking scheme being analysed, and noting the capture cross-sections of the dominant trap species, the electron density can be converted to a probability of capture if a trap was to be found at each individual mesh point. Integrating this probability of capture and normalising across the entire volume allows the calculation of a parameter that can be compared to different device geometries to allow a comparison of the predicted impact of any design changes on the capture of signal charge by traps and hence the charge transfer efficiency. Using this improved method allows the variation in electron density across the charge cloud to be fully integrated into the simulations of the impact of radiation damage on different device designs.

2017 JINST 12 C12021

5 Predicting the performance characteristics of a CCD for the SMILE SXI

As an example of the method described in section 4, we can consider the development of a CCD towards the SMILE SXI. To avoid any confusion regarding the current status of the SMILE SXI CCD development at the time of writing, we will consider arbitrary dose levels and use this as an example only of the methods that are presented and the overall aim of this paper and they should not be considered indicative of, for example, the end of life performance of the SMILE SXI.

A standard PLATO-like CCD [22, 23] would have the benefits to the SMILE SXI of a large area with only two readout nodes requiring electronics to be provided. A smaller CCD, such as that used for the Euclid VIS instrument for example, would require a larger number of CCDs to cover the same area of focal plane and hence would have greater requirements in terms of the electronics required to read out the images from the CCDs. However, given the size of the devices, a large number of transfers from pixel-to-pixel are required and hence the impact of radiation damage is increased; if the CTE was the same for two similar CCDs requiring different numbers of transfers, the CCD with the larger number of transfers would lose more signal, resulting in an effective increase in noise on the output signal. One method to reduce the impact of an increased number of pixel-to-pixel transfers is to reduce the width of the channel, or to introduce a Supplementary Buried Channel (SBC), such as that used in the GAIA CCDs [24].

We will consider here the parallel channels, using the initial buried channel width of 14 μm as our starting point to later compare the performance of design modifications. Narrowing the width of the buried channel will confine the signal electrons to a smaller width of silicon in one dimension, but this alone does not guarantee a lower probability of capture; above, we have already discussed the analogy to squeezing an inflated balloon in one dimension (resulting in an increase in width in another dimension), but here we must also consider the increase in the electron density from a reduced confinement volume (the number of electrons being the same but in a smaller volume). A change in the width of the buried channel results in a change in the amount of dopant present and this therefore has an impact on the depletion depth in the device. The depletion depth can be normalised to the 14 μm case through a higher dopant level being used to form the buried channel whilst maintaining the same width. We will consider three options here for simplicity: the original 14 μm channel width and two versions of a 4 μm channel (one with the same dopant concentration as the original device and one with an altered dopant level, designed to match the depletion depth to the 14 μm case). We shall refer to these three options as the 14 μm case, 4 μm case and the 4 μm *adj* (for 'adjusted' dopant level), figure 3.

Simulations of each pixel case were implemented in the Silvaco ATLAS toolkit at increasing signal levels over the range of a few electrons to several tens of thousands of electrons, approximately evenly spaced logarithmically. For each pixel and each signal level, the same evenly spaced mesh (covering the whole pixel volume) was used and electron densities interpolated to the evenly spaced mesh points. At each mesh point and for each signal level, the properties of the dominant trap species (for the temperature and timings under which the CCD would be operated) were used to calculate the probability of trapping during one clocking cycle (i.e. when signal charge was held within the pixel). Using these data, a sum of the probability of capture across the whole pixel could be calculated at each signal level and for each pixel structure; we refer to this as the *summed probability of capture*. Provided the same mesh is used for all arrangements, normalisation of the

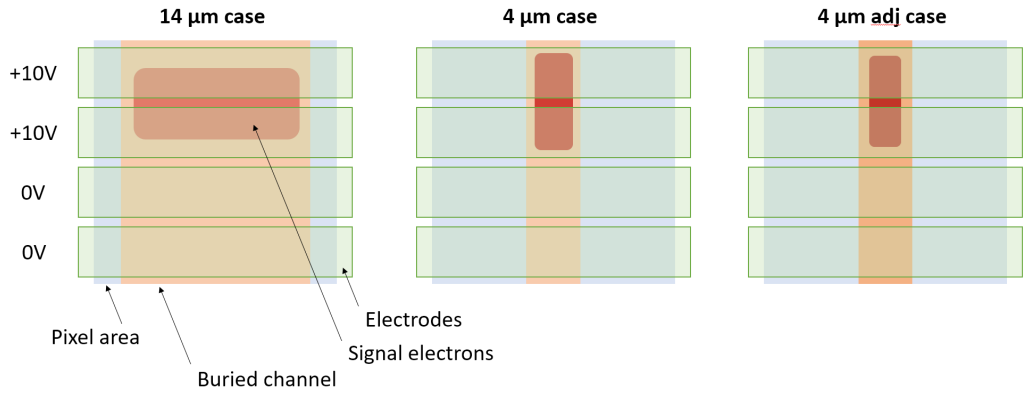

Figure 3. A cartoon of the three different cases considered, showing the 14 μm case and the two versions of the 4 μm channels. The difference between the 4 μm case and the 4 μm *adj* case is only the dopant concentration in the channel (changed to provide the same depletion depth as the 14 μm case in the *adj* geometry).

summed probability of capture is not required as the aim here is to compare the predicted results (i.e. it is the ratio of the summed probability of capture for each pixel case with the standard, known, device with the 14 μm channel).

To ensure the mesh suitably samples the volume of the pixel and that the results are not skewed by the location of the mesh points, a series of meshes of different mesh-spacing were tested and compared. The distance between mesh points can be halved and the summed probability of capture recalculated for each arrangement. As the mesh spacing is reduced the summed probability of capture will of course increase due to more points being sampled, however, if the relative variation across signal levels remains the same (i.e. within a few percent variation) after a reduction in the mesh spacing then this implies that the mesh is suitably fine such that no further mesh spacing reduction is required. In this way, a calculation of the change in summed probability of capture can be calculated for varying signal levels across the different pixel designs, figure 4.

Taking the summed probability of capture, which now incorporates any change in electron density in the calculation by design, it is possible to interpolate to all signal levels and produce the factor by which a change in pixel design will impact the device's ability to withstand radiation damage, figure 5. This factor of improvement is calculated across the energy range of interest and indicates how the device would be expected to perform across a range of energies.

We can now consider how the process above can help to determine device performance in a more detailed way. A standard measurement technique to compare device performance is that of X-ray CTI at a fixed energy (nominally using an Fe-55 source at a little below 6 keV for CCD characterisation, such as in [9]). With this one measurement on the 14 μm device, we can now predict the performance across all energies and all device variants. In this way, we can predict how a device might perform before the expensive process of full design and manufacture has taken place. In addition, other device parameters can be considered such as the readout noise and chosen event selection thresholds (e.g. 5σ above background noise) to examine the performance of the device in a mission-like situation at various stages of the mission. Two examples of performance predictions are given below to demonstrate the technique.

2017 JINST 12 C12021

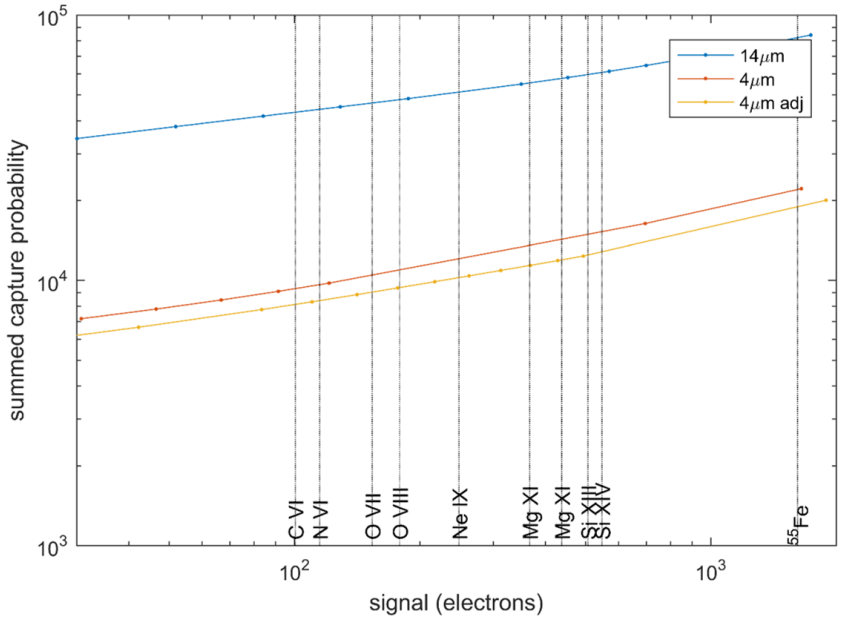

Figure 4. For the differing pixel designs, the summed probability of capture can be calculated and compared. Spectral line energies are shown to allow comparison for different science cases.

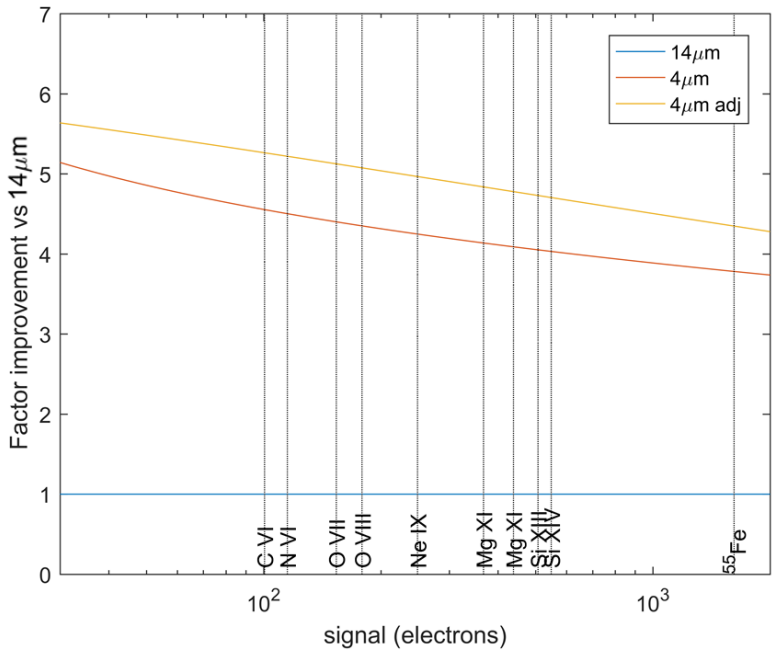

Figure 5. Factor of improvement in total charge that would be captured at different signal levels for the different pixel designs. Spectral line energies are shown to allow comparison for different science cases.

In order to determine the impact of the changes in pixel geometry and readout noise we must implement a Monte Carlo simulation of charge transfer through a CCD. Due to the large number of transfers required through the device, we use a pixel-to-pixel transfer in the device, using the current signal size and the information from figure 5 to recalculate the appropriate charge transfer efficiency (at and for each step) from the fixed CTI at Fe-55. The process is repeated for each transfer through the device, recalculating the new signal size at each transfer and using this new signal size to calculate the new effective charge transfer efficiency for the next step. In this way, the signal charge packet will gradually reduce in size and number of electrons as it is transferred through the device. A charge packet of any size can be initiated in any location in the CCD such that the signal size at the output node can be calculated. In practice, and for the examples presented below, we have considered all signal sizes from 1 to 2000 electrons across a grid of 20×20 positions evenly spaced across the device. These can then either be considered independently to examine the performance across different regions of the device, or they can be averaged to get a total performance across the whole device.

Firstly, let us consider the detectability of X-rays of different energies across each device variant following receipt of the same radiation dose, chosen for demonstration purposes only. From a single Fe-55 X-ray CTI measurement, we can predict the variation in area of device over which a range of energies of X-ray can be observed above the 5σ limit. We consider here an initial CTI level at Fe-55 of 5×10^{-5} for parallel transfers and 2×10^{-5} for serial transfers, based on the CTI that one might experience for a fluence of approximately 4×10^9 protons/cm^2 (10 MeV equivalent). An X-ray of low energy, and therefore generating few electrons, will lose a certain number of these electrons to traps during transfer (dependant on the CTI for the device) and this signal loss may leave the charge packet with insufficient signal to be over the 5σ limit above the background noise. Figure 6 shows the minimum X-ray energy that would be detectable in different locations of each device case, noting that the location of interaction on the CCD determines the number of transfers required (with more transfers meaning more signal lost to traps).

It is clear from figure 6 that the reduction in the width of the channel has an impact on the area of the device over which the lower energy X-ray events can be detected, but this does not tell us how the spectral performance will be impacted; if the number of signal electrons reaching the output is reduced but the readout noise remains the same then not only will the noise on the signal itself be larger as a fraction of the signal, but the readout noise will be larger as a fraction of the signal. We can now consider the spectrum that will be produced across the whole area of the device for which X-rays can indeed be detected, thus affecting both the width of the spectral lines and the intensity, figure 7.

6 Conclusions

In previous studies for which the device transfer times are relatively long and the signals large, a scaling based on the outer limits of the charge cloud has been demonstrated as a suitable approximation to the changes that are observed through a device geometry change. However, for lower signal levels and faster clocking, the probability of a trap capturing a signal electron can no longer be considered to be one where signal is present.

Using in-depth simulations of the pixel designs of current CCDs, one can vary the pixel geometry to test the improvement in performance with respect to radiation damage and CTI that can be predicted and help to guide the detector choices for future design and manufacture. Through a con-

2017 JINST 12 C12021

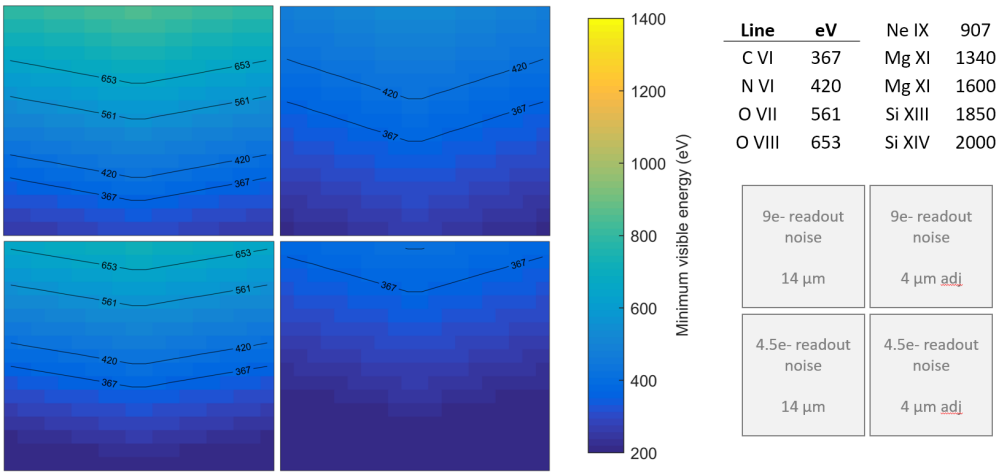

Figure 6. Signal electrons are transferred down through the device (4510 parallel transfers) and then to the left or right (2255 serial transfers) for the left and right halves of the CCD respectively. The minimial detectable energy is the smallest signal for which the number of signal electrons remains above the 5σ detection threshold. Different designs and readout noise levels can be considered for comparison at the radiation dose level, here showing two readout noise levels of 9 electrons rms and 4.5 electrons rms (change in output node) and the 14 μm and the 4 μm adjusted dopant cases (shown to allow comparison of worst-case, top-left, and the best case, bottom-right).

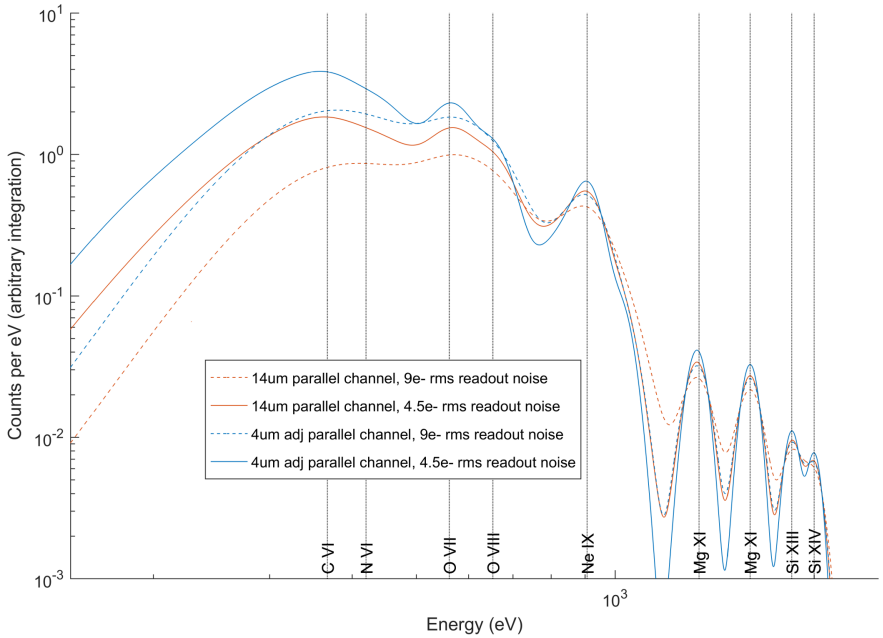

Figure 7. The spectral performance of the device is considered for this single radiation dose level across the best-case and worst-case pixel designs (14 μm and 4 μm adj) and output amplifiers (readout noise of 9 electrons rms and 4.5 electrons rms). The improvements to the both spectral line width (and therefore how resolvable the lines are) and the total count rates can be compared.

2017 JINST 12 C12021

sideration of the trap properties and electron density for each pixel geometry, the performance can be scaled for use in the faster-readout, lower-signal regime where the probability is less than one across the pixel. In these cases it is vital to take into account the varying electron density across the pixel.

Combining the results of the Silvaco ATLAS simulations with a small number of experimental results for a pre-existing device, one can predict the device performance, both from imaging area reduction due to signal loss from traps, and from the spectra that will be produced. In this way, vital decisions on device design to counteract radiation damage that may be experienced in-orbit can be made before the process of device design and manufacture.

Acknowledgments

With thanks to David Burt, formerly of *Teledyne e2v*, for general discussion. With thanks to the Science and Technology Facilities Council and U.K. Space Agency for their funding of the projects that have led to the development of the new techniques presented here.

References

[1] W. Shockley and W.T. Read Jr., *Statistics of the recombinations of holes and electrons*, *Phys. Rev.* **87** (1952) 835.

[2] R.N. Hall, *Electron-hole recombination in germanium*, *Phys. Rev.* **87** (1952) 387.

[3] D. Hall, J. Gow, N. Murray and A. Holland, *Optimisation of device clocking schemes to minimise the effects of radiation damage in charge-coupled devices*, *IEEE Trans. Electron Dev.* **59** (2012) 1099.

[4] A. Clarke, D. Hall, N. Murray, A. Holland and D. Burt, *Device modelling and model verification for the Euclid CCD273 detector*, *Proc. SPIE* **8453** (2012) 84531I.

[5] W. Raab et al., *SMILE: A joint ESA/CAS mission to investigate the interaction between the solar wind and Earth's magnetosphere*, *Proc. SPIE* **9905** (2016) 99052.

[6] D. Hall and A. Holland, *Space radiation environment effects on X-ray CCD background*, *Nucl. Instrum. Meth.* **A 612** (2010) 320.

[7] D. Hall, A. Holland and M. Turner, *Modelling instrument background for CCD X-ray spectrometers in space*, *Proc. SPIE* **6686** (2007) 66860J.

[8] D. Burt et al., *Improving radiation tolerance in e2v CCD sensors*, *Proc. SPIE* **7439** (2009) 743902.

[9] J.P.D. Gow, N.J. Murray, A.D. Holland and D. Burt, *Proton damage comparison of an e2v technologies n-channel and p-channel CCD204*, *IEEE Trans. Nucl. Sci.* **61** (2014) 1843.

[10] D. Wood et al., *Evolution and impact of defects in a p-channel CCD after cryogenic proton-irradiation*, *IEEE Trans. Nucl. Sci.* **99** (2017) 2814.

[11] J.R. Janesick, *Scientific charge-coupled devices*, SPIE Press (2001).

[12] D. Hall, N. Murray, A. Holland, J. Gow, A. Clarke and D. Burt, *Determination of In Situ Trap Properties in CCDs Using a "Single-Trap Pumping" Technique*, *IEEE Trans. Nucl. Sci.* **61** (2014) 1826.

[13] D.J. Hall, D. Wood, N. Murray, J.P.D. Gow, A. Chroneos and A. Holland, *In situ trap properties in CCDs: the donor level of the silicon divacancy*, 2017 *JINST* **12** P01025.

2017 JINST 12 C12021

[14] D. Wood et al., *A study of the double-acceptor level of the silicon divacancy in a proton irradiated n-channel CCD*, *Proc. SPIE* **9915** (2016) 99150J.

[15] R. Massey, C. Stoughton, A. Leauthaud, J. Rhodes, A. Koekemoer, R. Ellis et al., *Pixel-Based Correction for Charge Transfer Inefficiency in the Hubble Space Telescope Advanced Camera for Surveys*, *Mon. Not. Roy. Astron. Soc.* **401** (2010) 371 [arXiv:0909.0507].

[16] R. Massey, T. Schrabback, O. Cordes, O. Marggraf, H. Israel, L. Miller et al., *An improved model of Charge Transfer Inefficiency and correction algorithm for the Hubble Space Telescope*, *Mon. Not. Roy. Astron. Soc.* **439** (2014) 887 [arXiv:1401.1151].

[17] A. Clarke, D. Hall, N. Murray, J. Gow, A. Holland and D. Burt, *Pixel-level modelling and verification for the EUCLID VIS CCD*, *Proc. SPIE* **8860** (2013) 88600V.

[18] A. Clarke, D. Hall, A. Holland and D. Burt, *Modelling charge storage in Euclid CCD structures*, 2012 *JINST* **7** C01058.

[19] J. Endicott et al., *Charge-coupled devices for the ESA Euclid M-class Mission*, *Proc. SPIE* **8453** (2012) 845304.

[20] *ATLAS User's Manual*, vols. 1–2, software version 5.6.0.R, Silvaco International, Sunnyvale, CA (2003).

[21] D.J. Hall, A. Holland, N. Murray, J. Gow and A. Clarke, *Modelling charge transfer in a radiation damaged charge coupled device for Euclid*, *Proc. SPIE* **8453** (2012) 845315.

[22] T. Prod'homme et al., *Technology validation of the PLATO CCD at ESA*, *Proc. SPIE* **9915** (2016) 99150U.

[23] P. Verhoeve et al., *Optical and dark characterization of the PLATO CCD at ESA*, *Proc. SPIE* **9915** (2016) 99150Z.

[24] G.M. Seabroke, T. Prod'homme, N.J. Murray, C. Crowley, G. Hopkinson, A.G.A. Brown et al., *Digging supplementary buried channels: investigating the notch architecture within the CCD pixels on ESA's Gaia satellite*, *Mon. Not. Roy. Astron. Soc.* **430** (2013) 3155 [arXiv:1302.1873].

2017 JINST 12 C12021